

# A sustainable cellulose bioplastic film with extraordinary mechanical performance regenerated by vapor-induced phase separation

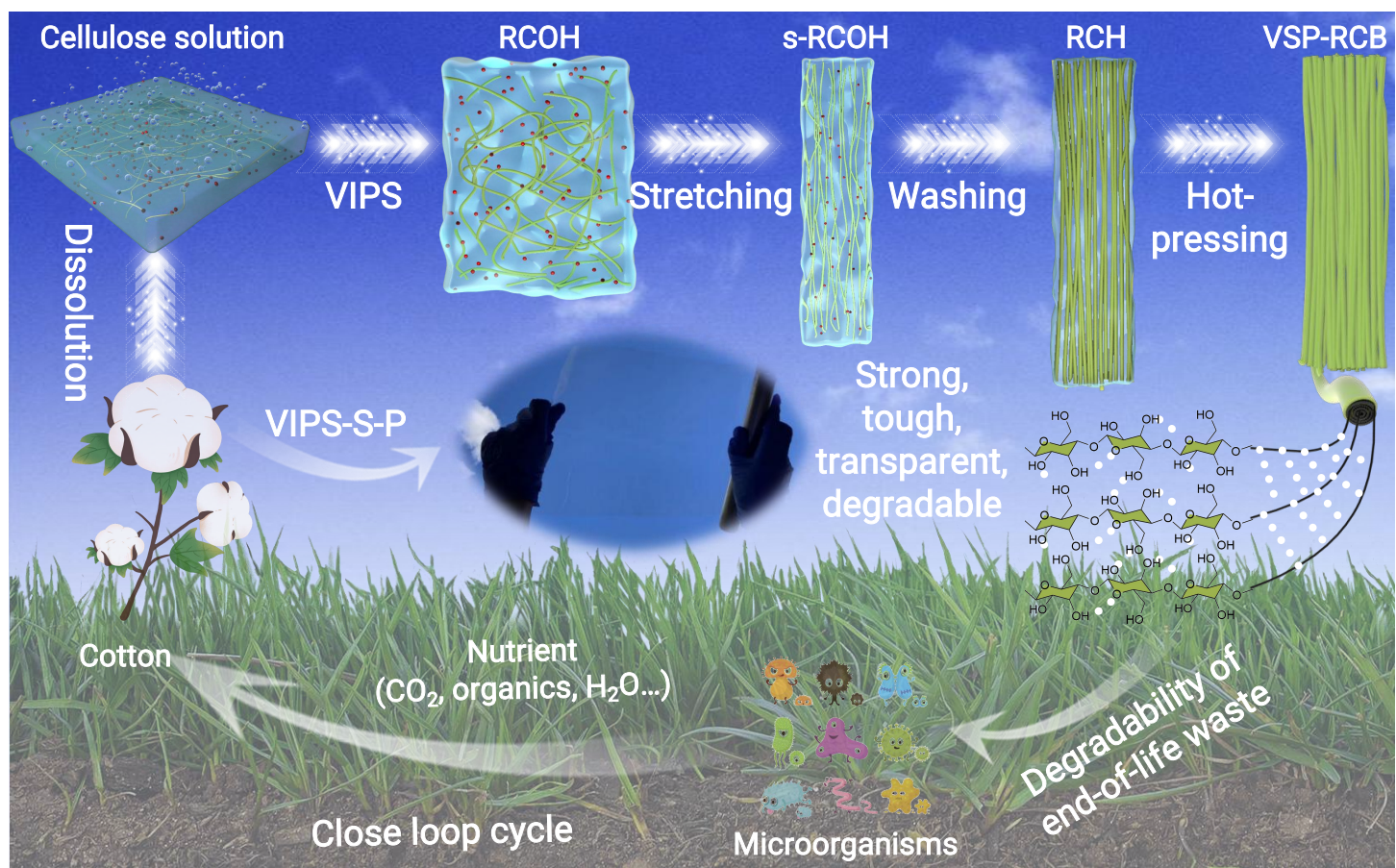
Hong Zhao, 1,2,3 Gui-Chun Hu, Brett Abraham, Qing Wang, Na Zhong, Fei Shen, Li-Hui Xu, Qun Yang, Piotr Batys, Qing-Shi Tu, Wojciech Płaziński, 5,7,\* Xian-wei Cheng, Zai-Sheng Cai, X and Jin-Guang Hu.

\*Correspondence: wojtek\_plazinski@o2.pl (W.P.); zshcai@dhu.edu.cn (Z.C.); jinguang.hu@ucalgary.ca (J.H.)

Received: October 15, 2024; Accepted: May 6, 2025; Published Online: May 12, 2025; https://doi.org/10.59717/j.xinn-mater.2025.100133

© 2025 The Author(s). This is an open access article under the CC BY license (https://creativecommons.org/licenses/by/4.0/).

# **GRAPHICAL ABSTRACT**



## **PUBLIC SUMMARY**

- A streamlined Vapor-Induced Phase Separation-stretching-hot-pressing (VIPS-S-P) is firstly proposed.
- A regenerated cellulose bioplastic (VSP-RCB) is produced by VIPS-S-P.
- The supramolecular assembly mechanisms of cellulosic network are revealed.
- This VSP-RCB showcases exceptional mechanical strength in wet and dry conditions.





# A sustainable cellulose bioplastic film with extraordinary mechanical performance regenerated by vapor-induced phase separation

Hong Zhao, 1,2,3 Gui-Chun Hu, 1 Brett Abraham, 1 Qing Wang, 1 Na Zhong, 1 Fei Shen, 4 Li-Hui Xu, 2 Qun Yang, 2 Piotr Batys, 5 Qing-Shi Tu, 6 Wojciech Płaziński, 5,7,\* Xian-wei Cheng, 8 Zai-Sheng Cai, 3,\* and Jin-Guang Hu,1,\*

Department of Chemical & Petroleum Engineering, University of Calgary Schulich School of Engineering, Calgary, Alberta T2N 1N4, Canada

<sup>2</sup>School of Textiles and Fashion, Shanghai University of Engineering Science, Shanghai, 201620, China

<sup>3</sup>Key Lab of Science & Technology of Eco-textile, Ministry of Education, College of Chemistry and Chemical Engineering, Donghua University, Shanghai 201620, China <sup>4</sup>Institute of Ecological and Environmental Sciences, Sichuan Agricultural University, Chengdu 611130, China

<sup>5</sup>Jerzy Haber Institute of Catalysis and Surface Chemistry, Polish Academy of Sciences, Niezapominajek 8, PL-30239 Krakow, Poland

Department of Wood Science, Faculty of Forestry, The University of British Columbia, Vancouver, BC V6T 1Z4, Canada

Department of Biopharmacy, Faculty of Pharmacy, Medical University of Lublin, Chodźki 4A, PL-20093 Lublin, Poland

<sup>8</sup> Jiangsu Engineering Research Center of Textile Dyeing and Printing for Energy Conservation, Discharge Reduction and Cleaner Production, Soochow University, Suzhou 215123, China

\*Correspondence: wojtek\_plazinski@o2.pl (W.P.); zshcai@dhu.edu.cn (Z.C.); jinguang.hu@ucalgary.ca (J.H.)

Received: October 15, 2024; Accepted: May 6, 2025; Published Online: May 12, 2025; https://doi.org/10.59717/j.xinn-mater.2025.100133

© 2025 The Author(s). This is an open access article under the CC BY license (https://creativecommons.org/licenses/by/4.0/).

Citation: Zhao H., Hu G-C., Abraham B., et al. (2025). A sustainable cellulose bioplastic film with extraordinary mechanical performance regenerated by vapor-induced phase separation. *The Innovation Materials* 3:100133.

We urgently need eco-friendly alternatives to non-biodegradable petrochemical plastics. Our study introduces a streamlined Vapor-Induced Phase Separation (VIPS) process, followed by stretching and hot-pressing (VIPS-S-P), to produce a regenerated cellulose bioplastic (VSP-RCB). This bioplastic showcases exceptional mechanical strength in wet and dry conditions, water stability, transparency, biocompatibility, biodegradability, and thermal stability. The scalable VIPS process involves cellulose dissolved in DMAc-LiCl coagulating with atmospheric water vapor to form a transparent organohydrogel (RCOH). The RCOH is aligned through stretching and densified via hot-pressing, creating a fully recyclable product from diverse cellulose sources. Molecular dynamics simulations and life-cycle assessment (LCA) explain RCOH generation mechanisms and environmental impacts. The VIPS-S-P strategy provides a sustainable approach to producing robust, transparent, water-stable, and biodegradable cellulose-based bioplastics, offering a compelling alternative to petrochemical plastics.

### INTRODUCTION

Despite the environmental issues and feedstock uncertainties associated with petrochemical-based plastics, the global demand for single-use plastics is on the rise. To address this, replacing conventional plastics with environmentally friendly and high-performance materials, commonly referred to as "bioplastics", offers a sustainable alternative. Cellulose, a natural polymer derived from plant photosynthesis with an annual yield exceeding 75 billion tons globally, represents an abundant and renewable resource. Additionally, the densely distributed hydroxyl groups in cellulose's molecular structure enable it to have a theoretical specific modulus and tensile strength higher than most synthetic polymers at the nanoscale. However, translating these exceptional nanoscale mechanical properties to macroscale cellulose films proves challenging due to numerous nanoscale defects, hindering the fundamentally nonideal stress transfer from the molecular to the macroscale.

The mechanical properties of cellulose films, crucial for their performance, are intricately linked to their micro-nano structure, determined by the film generation process. Researchers have employed "top-down" and "bottom-up" strategies, along with techniques like materials hybridization, fiber alignment, covalent cross-linking, and densification to create high-performance cellulose films. Although films directly fabricated from natural resources or extracts can achieve exceptional mechanical strength (up to 1 GPa) and stiffness (up to 55 GPa), they often exhibit brittleness (maximum strains of 5%), low toughness, and poor water stability. Whereas, regenerated cellulose films from dissolved cellulose in solvent systems (e.g. N-Methylmorpholine-N-Oxide, facid aqueous, finorganic salt solution, foinic liquids, N, N-dimethylacetamide/LiCl (DMAc/LiCl), alkali/urea aqueous, etc.) offer good strain (>10%), toughness and water stability, but accompany with a relatively lower strength (<550 MPa) and stiffness (<20 GPa). Therefore, generating cellulose films with desirable mechanical properties in both

wet and dry conditions for bioplastic applications remains a pervasive challenge.  $^{7}$ 

Vapor-induced phase separation (VIPS) has been successfully utilized in fabricating films from petrochemical-based polymers such as polyvinylidene difluoride, polysulfone, and polyethersulfone. VIPS provides greater control over mass transfer and polymer aggregation rates than other phase inversion methods due to the slower kinetics of gaseous non-solvents in comparison to liquid non-solvents. Notably, VIPS has not been applied to cellulose-based film generation to the best of the author's knowledge. Additionally, it has been demonstrated that the mechanical properties of cellulose films can be enhanced through fiber alignment and densification via mechanical stretching and hot-pressing. These combined techniques offer a novel platform for creating cellulose-based films with tunable morphology and improved mechanical properties.

Herein, we introduce a streamlined Vapor-Induced Phase Separation process coupled with stretching and hot-pressing (VIPS-S-P) to produce a regenerated cellulose bioplastic (VSP-RCB) from a cellulose/DMAc/LiCl solution. VSP-RCB demonstrates record-high strength, toughness, and stiffness in wet and dry conditions, along with excellent transparency, recyclability, and biodegradability. The process is universally applicable to various cellulose feedstocks (e.g., bacterial cellulose, dissolving pulp, hardwood pulps, and softwood pulps), and the DMAc/LiCl solvent system is recyclable. LCA indicates lower environmental impacts for VSP-RCB compared to conventional thermoplastic acrylonitrile butadiene styrene (ABS). We envision this transparent cellulose film as a sustainable replacement for widely used petrochemical-based plastics, offering exceptional mechanical performance in diverse conditions.

## **MATERIALS AND METHODS**

#### Materials and chemicals

Absorbent cotton ball, softwood pulp, hardwood pulp, dissolving pulp, and bacterial cellulose were used for the fabrication of VSP-RCB. Absorbent cotton ball was bought online. Softwood pulp and hardwood pulp were provided by Chenming Paper Mill (Weifang, China). Dissolving pulp was provided by generous CelluForce Inc. (Montreal, Canada). Bacterial cellulose was cultured according to the reported methods.<sup>25</sup> N, N-Dimethylacetamide (DMAC, ≥99.5%, HiPerSolv CHROMANORM® for HPLC, VWR) and anhydrous lithium chloride (LiCl, VWR) were used for dissolving the cellulose raw materials.

## **Preparation of DMAc/LiCl solution**

A 1:10 weight ratio of LiCl and DMAc was magnetically stirred at room temperature until a homogeneous and transparent liquid was obtained for use.

# Fabrication of the cellulose organohydrogels and bioplastics

Freeze-dried cellulose raw materials and DMAc/LiCl solution at a mass

ratio of 1:99 were mixed and sealed in a glass bottle. After being stirred at 150°C for 1 h, the glass bottle was continuously magnetically stirred at room temperature until a transparent cellulose/DMAc/LiCl solution was obtained. The resultant cellulose solution was transferred into the uncovered glass box cellulose solution to give a thickness of 0.80-1.0 mm and kept in a constant temperature and constant humidity laboratory (25°C and different relative humidity) to form the transparent organohydrogel (RCOH). For comparison, different processes were applied to fabricate the bioplastics. (1) After washing with tap water, the transparent hydrogel (RCH) was directly freeze-dried and obtained a white bioplastic which was denoted as V-RCB. (2) The transparent bioplastic was obtained by treating RCOH in the sequence of stretching, washing and lyophilization and named VS-RCB. (3) RCH went through a hot-pressing process which sandwiched the RCH between stainless plates and then dried at 80°C at an applied pressure of about 1 MPa. Finally, a transparent bioplastic was acquired and denoted as VP-RCB. (4) After stretching, the washed gel was hot-pressed under conditions as (3). Here, the bioplastic was denoted as VSP-RCB. To further investigate the influence of the stretching ratio on mechanical properties, the organohydrogels were stretched by different ratios (0%-160%). Except for the stretching ratio, all the processes are the same as that of VSP-RCB. As a comparison, RCOH and corresponding films prepared by traditional liquid-induced phase separation (LIPS) method. Here, the cellulose/DMAc/LiCl solution was directly regenerated to RCOH by immersing in the water. Then, the LIPS-generated RCOH was hot pressed to a LIPS-generated film.

#### **Characterization methods**

The morphology of the samples was observed with a Hitachi Regulus 8230 High-Resolution Cold Field Emission Scanning Electron Microscopy (FESEM). Atomic force microscope (AFM) images were recorded on a Shimadzu SPM-9700 (Japan) using a silicon nitride probe (RTESP-300, BRUKER) with a tip radius of 2 nm, a spring constant of 40 N/m and a high resonance frequency of 300 kHz. 2D WAXS and SAXS measurements were performed on a Xeuss 2.0 HR SAXS/WAXS instrument from Xenocs (France). The collimation mode was the high flux mode (HF). The beam center x for WAXS and SAXS were 460 and 235 while corresponding beam center z were 333 and 325, respectively. The wavelength used was 0.154 nm, and a Pilatus 300K X-ray detector (2×2 µm with a pixel size of 172 µm) was employed to collect data. The sample-to-detector distances for WAXS and SAXS were calibrated to 88 mm and 2480 mm by Silver Behenate, respectively. The time of exposure was 300 s, and the 2D scattering images were analyzed with Foxtrot software from the Xenocs. Fourier Transform Infrared spectra (FTIR) were recorded by a Nexus 670 FTIR spectrometer over the range of 400-4,000 cm<sup>-1</sup>. Pore size distribution of cellulose bioplastics was measured by the ultra-filtration membrane porometer (GaoQ PSMA-10, GaoQ Functional Materials Co., Ltd., China). The density of samples was confirmed by the Excellence XS Analytical Balance (XS204, Mettler Toled, United States). And, corresponding porosity was calculated as well, which has been demonstrated in the Supplementary Information in detail. X-ray diffraction (XRD) spectra were recorded by an 18 KW rotating target X-ray diffractometer (D/max-2550VB, Rigaku, Japan) equipped with Cu-Ka radiation generated at 40 KV and 0.1541 nm of wavelength. Samples were scanned between 10° and 90° and were performed with a scanning speed of 0.02° min<sup>-1</sup>. XRD spectra were analyzed by Jade 6.0 and the crystallinity index (CrI, %) was calculated as well, whose details were in the Supplementary Information. The degree of polymerization (DP) of cellulose raw materials was measured according to ASTM D1795-13.26 The water contact angles of the VSP-RCB were measured using a contact angle meter (KRÜSS Contact Angle DSA30R, KRÜSS, Germany). The light transmittance of the cellulose films was measured by a double-beam UV-visible spectrophotometer (Mapada UV-P7, China) with a wavelength ranging from 200 to 800 nm. The thermostability was measured by a thermogravimetric (TG) analysis (CLARUS SQ8-STA8000, PerkinElmer, USA) using a heating rate of 10 °C min-1 in air. Tensile tests of the cellulose organohydrogel and bioplastics were performed on an INSTRON instrument (Model 5966, USA) equipped with pneumatic clamps to avoid slippage. The cellulose organohydrogels (thickness of 0.4-0.7 mm and width of 20 mm) were stretched at a speed of 10 mm min<sup>-1</sup>. The cellulose bioplastics (thickness of 10-300 µm and width of 3 mm) were stretched at a speed of 3 mm min<sup>-1</sup>.

#### Molecular modeling

The molecular modeling relied on molecular dynamics (MD) simulations carried out at all-atom (AA) or coarse-grained (CG) levels of resolution. See details in the Supplementary Information.

## **Biocompatibility test**

To assess the biocompatibility of the VSP-RCB as a potential scaffold in tissue engineering applications, human umbilical cord-derived Mesenchymal Stromal cells (hUC-MSCs) were cultured on top of the cellulose film for 5 days. See details in the Supplementary Information.

#### **Biodegradability test**

The VSP-RCB and polyethylene terephthalate (PET) were fixed on the soil 50 by pushpins and monitored regularly to test their biodegradability. Cellulose hydrolysis of VSP-RCB by cellulase enzymes. The enzymatic hydrolysis experiments were carried out at 2% (w/v) solids loading in sodium acetate buffer (50 mM, pH 4.8), 50°C, 150 rpm with 30 mg cellulase enzymes per gram of cellulose in a benchtop shaking incubator. Samples were periodically taken during hydrolysis, and the concentration of glucose in the supernatants was measured using HPLC. All hydrolysis experiments were performed in triplicate and mean values and standard deviations are presented.

#### Life-cycle assessment

LCA models were created for the bioplastics manufactured from cotton using the VIPS-S-P treatment process. The benchmark production for comparison was ABS. The functional unit of the LCA models took into consideration both the mass of the product (i.e., 1 kg) and its key properties (i.e., density and tensile strength). The system boundary was cradle-to-gate, including feedstock preparation and transportation, preparation of ancillary materials (e.g., DMAc/LiCl solution preparation), as well as energy consumption and waste generation during the manufacturing of the products. Accordingly, the delivery, use, and end-of-life treatment of the bioplastics and benchmark product were excluded from the analysis. The TRACI [v2.1, February 2014] life cycle impact assessment method was used to estimate the values of different impact categories (e.g., climate change impact in the unit of kg CO<sub>2</sub>-eq) for the LCA models. OpenLCA (version 1.10.3) and Ecoinvent® (version 3.7.1, cut-off system) were used to create these LCA models based on the inventory data. See details in the Supplementary Information.

#### **RESULTS AND DISCUSSION**

## VIPS regeneration of cellulose organohydrogel

This work presents a bottom-up approach to directly transform cellulose feedstock into a transparent cellulose film with exceptional mechanical performance. Cellulose dissolves in a DMAc/LiCl solvent system, and spontaneously coagulates with atmospheric water vapor through vapor-induced phase separation (VIPS), forming a transparent cellulose organohydrogel (RCOH) at the air-solvent interface. The RCOH undergoes stretching to induce an anisotropic fiber network structure (s-RCOH), followed by water washing to remove the DMAc/LiCl solvent shell, generating a wet cellulose hydrogel (RCH). Lastly, hot-pressing dries and densifies the RCH to produce the final regenerated cellulose bioplastic (VSP-RCB) (Figure S1).

Generally, during a phase inversion process, a molecularly homogeneous polymer solution is converted from a single phase into two phases which corresponds with a breaking of the thermodynamic equilibrium of the solution. In this work, the VIPS process disrupts the thermodynamic equilibrium of cellulose in DMAc/LiCl by introducing water from the air, offering slower and more controllable mass transfer rates than the commonly used liquidinduced phase separation (LIPS) method (Figure S2). 16,27 As a result, the VIPSgenerated RCOH exhibits a visibly smoother appearance and a denser microstructure, devoid of pores, microvoids, and macro voids (Figure S3).28 It demonstrates excellent mechanical performance, with a tensile strength of up to 4.05 MPa and a breaking point strain of up to 132.54% (Figure S4A). After hot-pressing, the cellulose film prepared via VIPS exhibits significantly enhanced mechanical properties compared to a LIPS-generated film, with 4.2 times higher tensile strength (210 MPa vs. 50 MPa), 11.2 times higher stiffness (5.6 GPa vs. 0.5 GPa), and 4.5 times higher toughness (59.8 MJ m<sup>-3</sup> v.s.

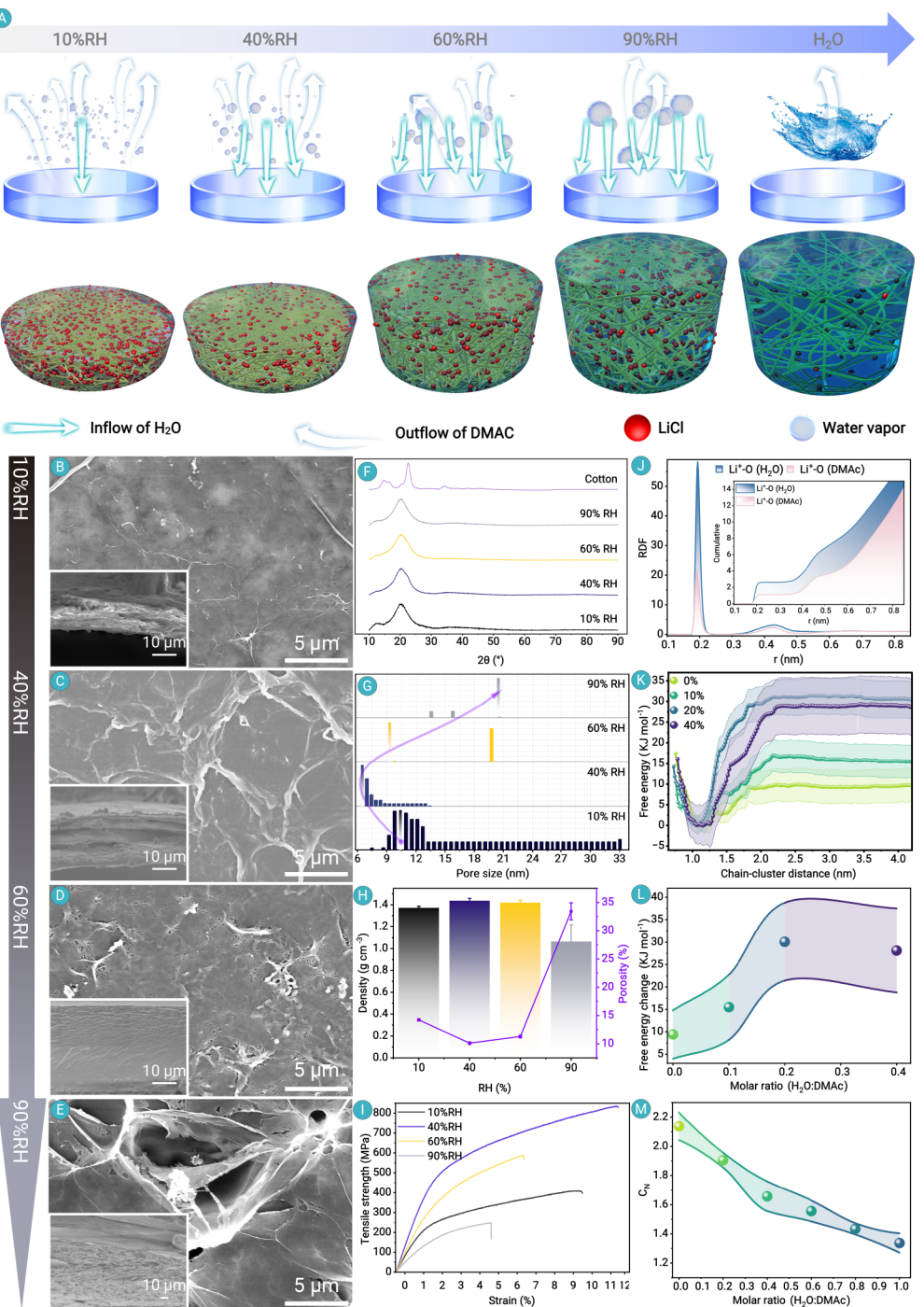


Figure 1. The VIPS regeneration of cellulose solution (A) The schematic diagram illustrating the mechanism of Vanor-Induced Phase Separation SEM of surface and corresponding cross-section of RCOH under different RH: (B) 10%, (C) 40%, (D) 60%, and (E) 90%. (F) XRD patterns, (G) pore size distribution, (H) density, and (I) the strain curves of RCOH under different RH. (J) The radial distribution function between Li+ and oxygen atoms in water and DMAc (the inset is the cumulative number of oxygen atoms). (K) Free energy profiles calculated for the process of aggregation of octameric chains to a surface of cellulose II cluster composed of 15 chains in DMAc/LiCl solvents containing various amounts of water (0%, 10%, 20%, and 40%) by umbrella sampling MD simulations. (L) Free energy differences between limiting states of aggregation of octameric chains calculated from the data shown in panel (K). (M) The average coordination number calculated for all CG beads representing either hydroxymethyl or diol moieties, obtained using cutoff 0.5 nm for different molar fractions of water (100%DMAc,40%H<sub>2</sub>O/60%DMAc,60%H<sub>2</sub>O/40%DMAc, and 100%H2O) in the system (Insets show the cluster structures obtained at 0 and 1 water molar frac-

ation sites. 830 The RCOH at 40% RH exhibits the smallest pore size distribution (6.5 nm) and the highest density (1.44 g cm<sup>-3</sup>) (Figures 1F-G), forming a tight anisotropic structure with the best mechanical properties of the conditions tested (Figures S3F & 2H).

During the VIPS process, DMAc and LiCl molecules migrate to assembled water from the air, leading to the self-assembly of new -OH groups on cellulose chains through intermolecular and intramolecular hydrogen bonds, forming RCOH (Figures S9A & S10).<sup>7</sup> Subsequently, it continuously shrinks in all dimensions until reaching equilibrium (Figures S9B-C & S11).

MD simulations are conducted according to the experimental composition (Table S1, Figure S12). The results of MD simulations and experiments reveal that cellulose molecules align and aggregate in the presence of solvent. The initial and final configurations of the cellulose cluster after 0.8 µs MD simulations are illustrated in Figures S13A-B, with its structure presented in Figure S13C. The rearrangement of hydrogen bonds in cellulose chains transforms the crystalline texture from cellulose I to cellulose II with anisotropic structure (Figures 1E, S3F, S13 & S14).

To understand the nature of the observed

cellulose aggregation, it is useful to consider LiCl interactions with system solvents (water and DMAc). The radial distribution function between Li<sup>+</sup> ions and solvent molecules reveals Li<sup>+</sup> ions' preference for water (Figure 1I). The water/DMAc ratio in the first coordination sphere of Li<sup>+</sup> indicates approximately 2.4 times higher affinity for water. Therefore, it can be concluded that the addition of water to the cellulose/DMAc/LiCl system alters the ion solvation shell, decreasing cellulose solubility by disrupting DMAc-Li<sup>+</sup> association, i.e. the factor recognized as essential for cellulose dissolution in DMAc/LiCl solutions.31 This effect is demonstrated by free energy changes associated with partial aggregation of cellulose II-like clusters in DMAc/LiCl solvents containing various amounts of water (Figures 1J-K). Any water addition raises the corresponding free energy level (by up to 20 kJ mol<sup>-1</sup> when referring to the detachment of a single octameric chain from the surface of a cluster composed of 16 chains), making the dissolution process less favorable. A qualitative insight into the MD trajectories confirms the existence of aggregation between Li<sup>+</sup> and water molecules. This simulation also explains

13.3 MJ m<sup>-3</sup>) (Figure S4B).

The VIPS process outlined here is driven by several different competing mass transfer processes, including DMAc evaporation, water absorption, and phase separation. The relative humidity (RH) of the surrounding air significantly influences water vapor mass transfer into the polymer solution (Figure 1A). Varied RH levels result in significant differences in the macroscopic structure, mass, volume, and water content of RCOH (Figures S5-S6). At 10% RH, DMAc evaporation dominates the process (Figure S7A), producing RCOH with dense structure and high LiCl content (Figures 1B & S5A). At 40% RH, a two-stage phenomenon occurs, initially driven by water absorption, later overtaken by DMAc evaporation (Figures S7B & S5B). Similar phenomena have also been observed in other polymer/solvent systems. While high humidity (60% RH and 90% RH) primarily relies on water absorption (Figures S7C-D), yielding RCOH with larger granular cellulose aggregates, higher porosity, and larger pores (Figures 1C-F & S8). Overall, higher RH results in larger and more numerous pores due to increased water molecule nucle-

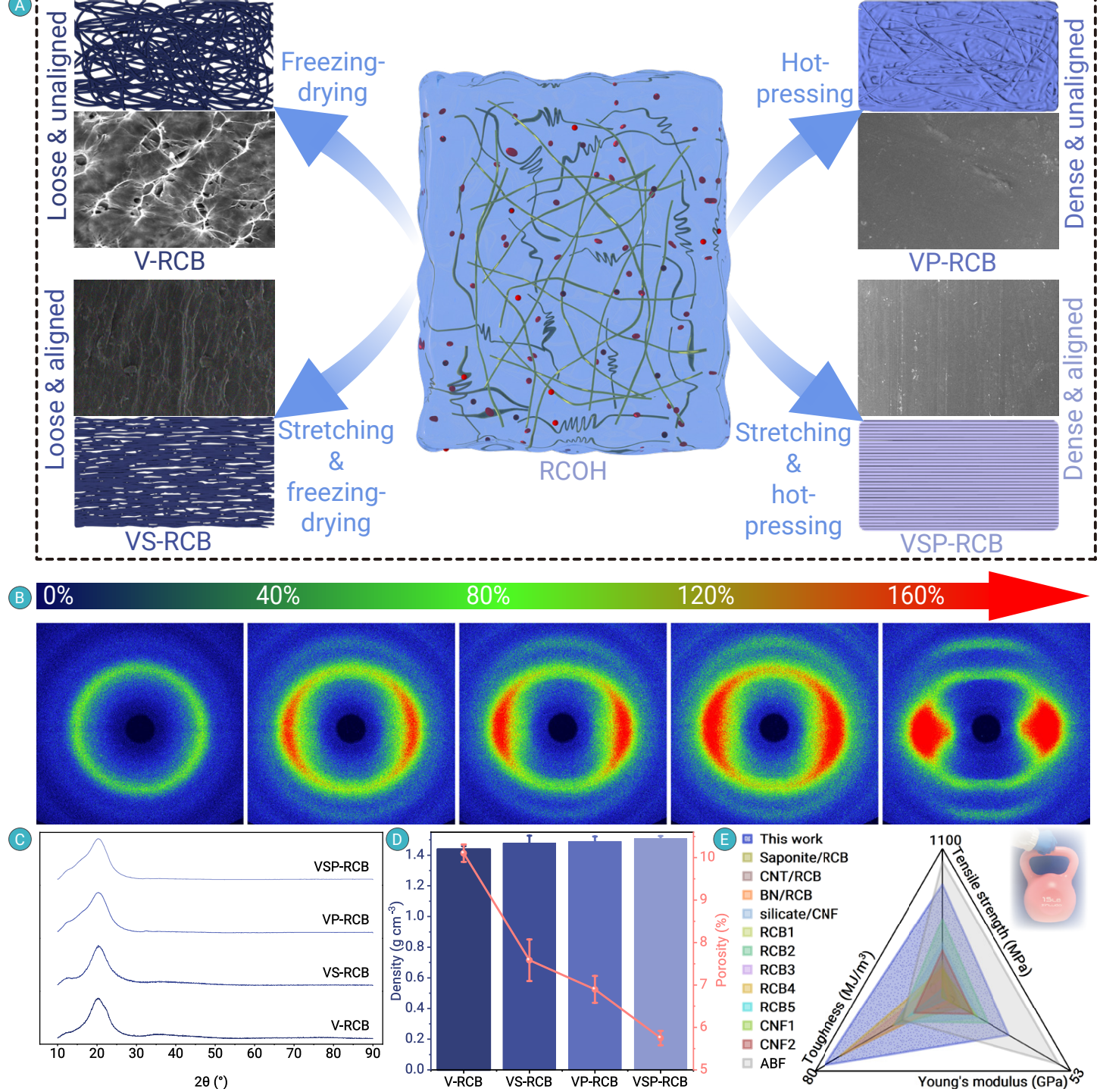


Figure 2. Well-ordered and densified nanostructure of VSP-RCB (A) The nanostructure illustrations of VSP-RCB prepared by the different processes. (B) 2D WAXS of the VSP-RCB prepared under different stretching ratios. (C) XRD patterns. (D) The density and porosity of films prepared by different processes. (E) The radar plot for the mechanical performance of VSP-RCB and other transparent cellulose-based films, including the aligned BC film, CNF films and its composites, regenerated cellulose films and its composites (the inset shows the VSP-RCB can lift a 15 lb kettlebell).

the experimental results theoretically, as the cellulose/DMAc/LiCl solution continuously absorbs moisture from the air and eventually regenerates into RCOH.

Coarse-grained (CG) MD simulations show that initially randomly displaced oligomeric chains tend to form aggregates, resembling cellulose II-like sheets with aliphatic patches on glucopyranose rings. These sheets may further aggregate into clusters resembling cellulose II crystal structure. The observed aggregation is a consequence of the lack of Li<sup>+</sup> ions, essential for the dissolution of cellulose but impossible to model at a sufficient degree of accuracy at the CG level. The degree of aggregation is highly dependent on the system,

and the solvent composition can be considered the main variable responsible for alterations in aggregation properties (Figures 1J-L). Figure 1M shows the systematic decrease in the average coordination number of polar CG beads, representing either hydroxymethyl or diol moieties present in cellulose chains, correlated with the increasing fraction of water in the system. The potency of self-aggregation of cellulose does not diminish completely but is significantly reduced upon the addition of water. According to the coordination number-based descriptor accepted here, and by assuming linear dependence, the loss of aggregation properties can roughly be estimated as equal to ca. 8% per 0.1 molar fraction of water in the system. Such change can

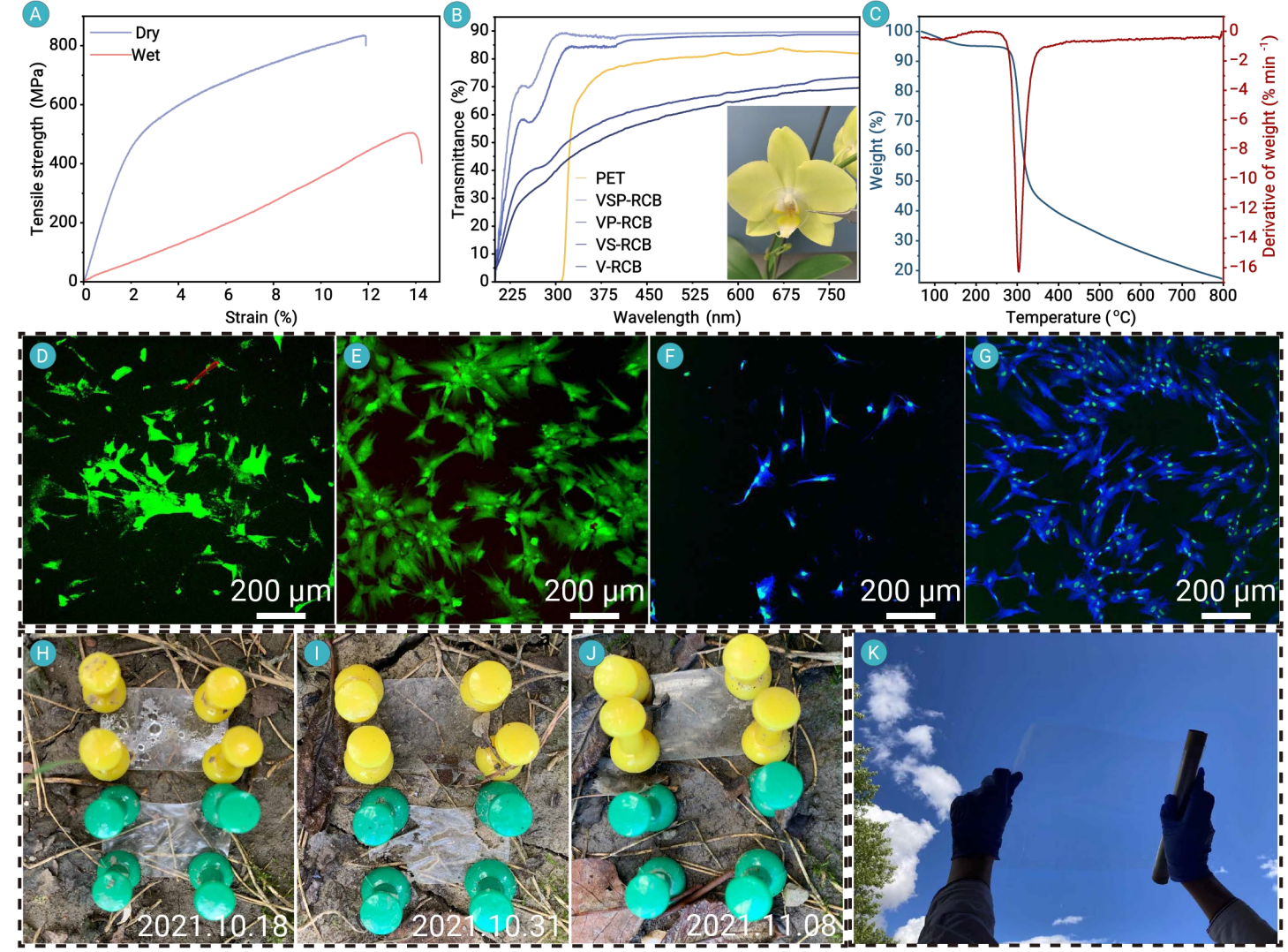


Figure 3. Water stability, optical property, thermal stability, and biocompatibility of VSP-RCB (A) The wet tensile strength, (B) the transmittance, (C) TG analysis and Derivative TG (DTG) curves of the VSP-RCB. (D)-(G) The confocal fluorescent images of hUC-MSCs grown on VSP-RCB: Live/Dead staining of hUC-MSCs on culture (D) day 1 and (E) day 5 (Green represents live cells, red represents dead cells). Cell nucleus and actin cytoskeleton staining of hUC-MSCs on culture (F) day 1 and (G) day 5. (H)-(J) Photos recording the process of degradation of the VSP-RCB: (H) 2021.10.18, (I) 2021.10.31, (J) 2021.11.08, (K) large-scale VSP-RCB with high transparency.

certainly affect the large-scale properties of formed cellulose aggregates, by e.g. increasing the solubility of chains of shorter lengths.

Throughout VIPS water competes with DMAc for Li+ and cellulose chains, affecting cellulose solubilization and chain assembly (Figure S15). All-atom (AA) MD simulation results show that the affinity of water for Li<sup>+</sup> is higher than that of DMAc for Li+, and that water "grabs" Li+ in the cellulose/ DMAc/LiCl solvation system, destroys the cellulose/DMAc/LiCl solvation system, and promotes the aggregation of cellulose chains, which ultimately leads to the formation of cellulose-like II aggregates. Different relative humidities lead to different water content in the final system (Figure S6D), different solvent solubilization capacities for cellulose, and different selfaggregation properties of cellulose depending on the water content and partially independent of water-Li<sup>+</sup> interactions. In summary, both AA and CG MD simulations show that water in DMAc-LiCl-cellulose solutions affects cellulose aggregation in two ways. Firstly, by introducing Li+-water interactions, competing with those driving cellulose dissolution under dry conditions. Secondly, by altering the chain-chain contact pattern during chain aggregation into cellulose II clusters.

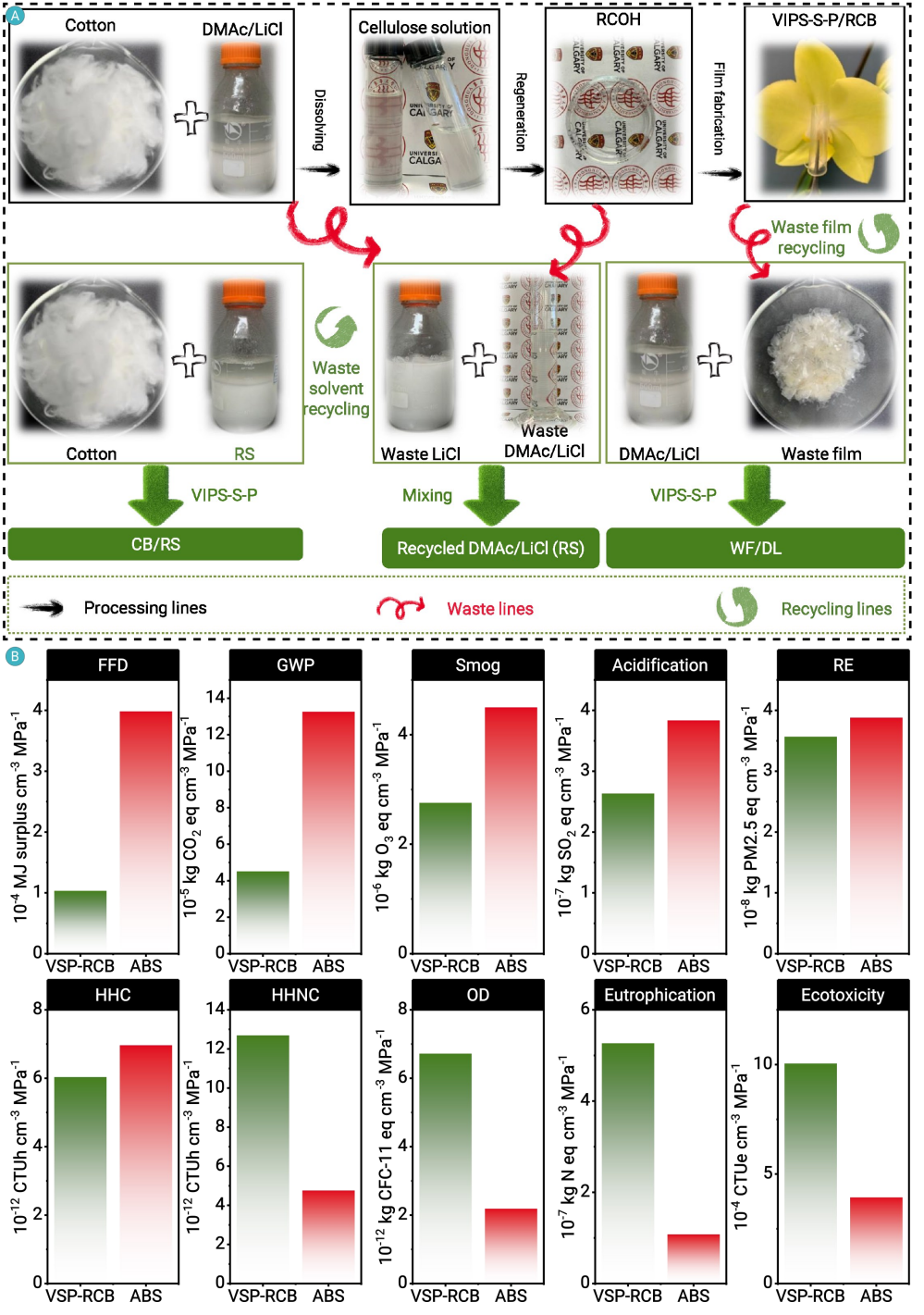
## Alignment and densification of cellulose nanostructure.

After VIPS regeneration, the RCOH was stretched and hot-pressed to create the ultra-strong regenerated cellulose bioplastic (VSP-RCB). As expected, The mechanical performance of VSP-RCB prepared at 40% RH

outperforms those prepared at other RH (Figure S16). Stretching and hotpressing primarily impact the alignment and densification, respectively, of the cellulose nanostructure, as indicated by WAXS, SAXS, XRD, degree of orientation ( $\Pi$ ), SEM, and AFM analysis (Figures 1A-C & S17-S18). VSP-RCB prepared with an increased stretching ratio exhibits elongated longitudinal 2D SAXS patterns and clear equatorial arcs in the WAXS patterns, indicating anisotropic properties through cellulose nanofiber alignment (Figures 2B & S19A). Additionally, the crystallinity index (CrI) and  $\Pi$  of the VSP-RCB increase from 66% to 86% and 57.5 to 76.0, respectively, under stretching (Figures 2C & S19B-C). SEM and AFM observations (Figures S17-S18) confirm the existence of a long-range aligned nanofiber architecture along the prestretching direction.

Pore size and density of the VSP-RCB were first reduced through stretching (Figures 2D & S20), and further with hot-pressing. Whereas the hot-pressing process also contributed to reducing the film's roughness. The maximum density achieved for the VSP-RCB was 1.51 g cm<sup>-3</sup>, close to the theoretical density of cellulose crystals (1.6 g cm<sup>-3</sup>).<sup>33-35</sup> This suggests the removal of most defects in the cellulose film, such as pores and cavities, during our treatment (Figure 2D).<sup>36</sup> This highly dense, layer-by-layer self-assembled anisotropic structure was also verified by SEM images of different axial planes of VSP-RCB (Figure S21).

Thanks to its high CrI, Π, density and nearly defect-free microstructure, VSP-RCB exhibited superior mechanical performance among the samples



VSP-RCB ABS

Figure 4. The sustainability of the VSP-RCB(A) The recycling strategy of waste DMAc/LiCl solvent and waste VSP-RCB. (B) Environmental impacts of the VSP-RCB compared to ABS (here are the abbreviations in the figure: FFD is "fossil fuel depletion", GWP is "global warming potential", RE is "respiratory effects", HHC is "human health-carcinogenics", HHNC is "human health-non-carcinogenics", OD is "ozone depletion").

66,42 and epoxy42 (Figure S24A). With a specific strength of 554 ± 25 MPa cm<sup>3</sup> g<sup>-1</sup>, it even outperforms materials such as densified wood (422 MPa cm<sup>3</sup> g<sup>-1</sup>), lightweight titanium alloy (244 MPa cm<sup>3</sup> g<sup>-1</sup>), and many alloys (Figure S24B). The mechanical properties of VSP-RCB are comparable to carbon and glass fiberbased composites used in vehicles.2 While its specific tensile strength is lower than aligned bacterial cellulose film (809 MPa cm<sup>3</sup> g<sup>-1</sup>), it excels in strain and toughness, crucial for bioplastic applications (strain of 4.4% and toughness of 25 MJ m<sup>-3</sup>). The bottom-up VSP-RCB process is universally effective for various cellulose materials, including bacterial cellulose, softwood pulp, dissolving pulp, and hardwood pulp, yielding impressive properties in all regenerated cellulose films (Figure S25).

#### The properties of VSP-RCB.

Our cellulose film underwent testing for essential bioplastic characteristics. Effective mechanical properties in wet conditions are crucial for the broad applicability of bioplastics. The stretching and hot pressing process not only enhanced its mechanical properties but also increased hydrophobicity, reflected in a higher water contact angle from 35° to 73° (Figure \$26),<sup>20,43</sup> VSP-RCB demonstrated remarkable tensile strength (~500 MPa), strains (13.7%), and toughness (35.6 MJ m<sup>-3</sup>) when wet, surpassing other cellulose films by an order of magnitude (Figure 3A, Table S3).36,44-

<sup>46</sup> The film's aligned cellulose nanofibers yielded a smooth surface and high transparency of 89.6%, exceeding PET (82.0%) (Figure 3B).<sup>27,36</sup> Thermogravimetric analysis showcased the film's excellent thermal stability with a decomposition temperature of 304°C (Figures 3C & S27). These outstanding properties position VSP-RCB as an ideal substrate for

but it can compromise the film when the strain at break is reached (Figure S23). Hot pressing, however, effectively mitigated the loss of strain with increasing tensile strength (Figure S22). Usually, strength and toughness are mutually exclusive in man-made materials, therefore, development of materials with both high strength and toughness remains a great challenge. 37-39 In our study, the VSP-RCB demonstrated both high strength and toughness. This is attributed to the significant reduction in intrinsic defects and increased stacking density of aligned cellulose nanofibers resulting from the combined effects of VIPS, stretching and hot pressing. Additionally, the enhanced frac-

tested (Figure S22). Increased stretching typically enhances tensile strength,

an increased spatial density of hydrogen bonds during interfacial sliding.<sup>7</sup> The cellulose film produced in this process outperforms common composite films, displaying mechanical properties superior to both isotropic and anisotropic cellulose composites (Figure 2E, Table S2). Notably, it also surpasses widely used plastics like polystyrene, 40 polyvinyl alcohol, 41 nylon

ture toughness is attributed to improved interfacial dissipation energy from

flexible electronic applications such as thin-film transistors, 47 organic lightemitting diodes, 48 foldable antennas, 49 or electroluminescent devices.5

To assess the biocompatibility of the VSP-RCB as a potential scaffold in tissue engineering applications, hUC-MSCs were cultured on cellulose film for 5 days. A Live/Dead stain was used to determine whether the film had cytotoxic effects on the growing cells. Very little cell death was seen on day 1 with the majority of cells attaching to the film with high viability. This high viability was maintained over five days of culture where the hUC-MSCs were able to proliferate on the scaffold with very little cell death observed (Figures 3D-E). A similar trend was also seen when staining for the actin cytoskeleton, where cells proliferated and migrated over the substrate and reached a high degree of confluency on the film (Figures 3F-G). These results indicate that VSP-RCB is non-cytotoxic, allowing cells to attach, proliferate, and migrate, making it a promising scaffold for tissue engineering applications.

Beyond that, the VSP-RCB also exhibited excellent biodegradability and scalability. When VSP-RCB and PET films were placed outdoors in a natural environment, the VSP-RCB was fully degraded in 3 weeks, while the PET film remained unchanged (Figures 3H-J). This highlights the film's composition of biomaterials that are readily degradable by microorganisms in normal environmental conditions. Further, treatment with a cellulase cocktail led to complete hydrolysis of VSP-RCB into glucose within 2 days (Figure S28). We next showcased the scalability of VSP-RCB production (Figures 3K & S29). The transparent cellulose/DMAc/LiCl solution was transferred into a large glass vessel. Subsequently, the VIPS process yielded a large transparent RCOH, which underwent stretching, washing, and hot-pressing to produce a sizable VSP-RCB film.

#### The sustainability of VIPS-S-P strategy.

To assess the recyclability of LiCl and DMAc after the VIPS-S-P process, we regenerated DMAc/LiCl solvent from the leftover "waste" and used it to dissolve cellulose for another round of bioplastic generation (CB/RS). Additionally, we evaluated the recyclability of the VSP-RCB by redissolving the endof-life VSP-RCB into DMAc/LiCl solution to regenerate new bioplastic (WF/DL) (Figure 4A). The tensile strength of WF/DL and CB/RS still reached 610 MPa and 596 MPa, respectively (Figure S30A). These mechanical properties remain outstanding among cellulose-based films, including CNC films, CNF films, bacterial cellulose films, wood-based films, commercial cellophane films, and regenerated cellulose films (Figure S30B).

A cradle-to-grave LCA was conducted to quantify the environmental impacts of the VSP-RCB, as compared to ABS (Figure S31, Table S4). The functional units of the LCA model consider both the mass of the product (i.e., 1 kg) and its key characteristics (i.e., density and tensile strength, Table S5). The VSP-RCB demonstrated lower environmental impacts than ABS in 6 of the 10 impact categories, primarily due to its superior tensile strength when incorporated into the functional unit (Figure 4B). Despite being a low-carbon alternative to ABS with a 30-66% reduction in global warming potential, VSP-RCB exhibited higher impacts in several other categories. Chemical production (for the DMAc/LiCl solution) and feedstock procurement were the main contributors. For example, in the "human health: non-carcinogenics" category, 59% and 35% of the impacts originated from the manufacturing of DMAc and LiCl and the procurement of cotton fiber, respectively. Similar patterns were observed for the "Ozone depletion", "Ecotoxicity" and "Eutrophication" categories. This emphasizes the importance of embodied impacts from materials, chemicals in particular, for the VSP-RCB.

In summary, the exceptional mechanical performance in both dry and wet states, transparency, water stability, biocompatibility, biodegradability, scalability, and recyclability collectively position the VSP-RCB as a promising candidate for next-generation sustainable and environmentally friendly bioplastics across various applications.

## CONCLUSION

In this work, we introduced a facile yet sustainable VIPS-S-P regeneration strategy for producing an ultrastrong, ultratough, transparent, hydrostable, scalable, biodegradable, and recyclable cellulose-based bioplastic. Cellulose dissolved in DMAc/LiCl was regenerated into a hydrogel (RCOH) with a dense nanostructure through water vapor absorption. Subsequent stretching and hot-pressing processes aligned and densified the cellulose nanostructure, yielding a cellulose bioplastic (VSP-RCB) with high density, crystallinity, and orientation. VSP-RCB exhibited outstanding mechanical performance: tensile strength (835.8 MPa), toughness (73.6 MJ m<sup>-3</sup>), and Young's modulus (27.5 GPa at dry state). This bioplastic is transparent, biodegradable, retains strength when wet, and the scalable manufacturing process accommodates various cellulose sources. Life cycle assessment demonstrated significantly lower environmental impact compared to petrochemical-based plastics like ABS. This approach offers a unique opportunity for crafting mechanically robust bioplastics from abundant, renewable, and sustainable biomass for a more eco-friendly future.

## **REFERENCES**

- 1. Brahney J., Hallerud M., Heim E., et al. (2020). Plastic rain in protected areas of the united states. *Science* **368**:1257–1260. DOI:10.1126/science.aaz5819
- Li T., Chen C., Brozena A.H., et al. (2021). Developing fibrillated cellulose as a sustainable technological material. Nature 590:47–56. DOI:10.1038/s41586-020-

#### 03167-7

- Wang Z., Xu C., Qi L., et al. (2024). Chemical modification of polysaccharides for sustainable bioplastics. *Trends Chem.* 6:314–331. DOI:10.1016/j.trechm.2024.04.009
- Zeng Z., Yu L., Yang S., et al. (2024). Tuning water-cellulose interactions via coppercoordinated mercerization for hydro-actuated, shape-memory cellulosic hydroplastics. *Matter* 7:3036–3052. DOI:10.1016/j.matt.2024.04.033
- Zhang L., Chen L., Wang S., et al. (2024). Cellulose nanofiber-mediated manifold dynamic synergy enabling adhesive and photo-detachable hydrogel for self-powered E-skin. *Nat. Commun.* 15:3859. DOI:10.1038/s41467-024-47986-y
- Habibi Y. (2014). Key advances in the chemical modification of nanocelluloses. Chem. Soc. Rev. 43:1519–1542. DOI:10.1039/C3CS60204D
- Ray U., Zhu S., Pang Z., et al. (2021). Mechanics design in cellulose-enabled highperformance functional materials. Adv. Mater. 33:2002504. DOI:10.1002/adma. 202002504
- Menut P., Pochat-Bohatier C., Deratani A., et al. (2002). Structure formation of poly (ether-imide) films using non-solvent vapor induced phase separation: Relationship between mass transfer and relative humidity. *Desalination* 145:11–16. DOI:10.1016/ S0011-9164(02)00323-5
- Mittal N., Jansson R., Widhe M., et al. (2017). Ultrastrong and bioactive nanostructured bio-based composites. ACS Nano 11:5148-5159. DOI:10.1021/ acsnano.7b02305
- Li K., Clarkson C.M., Wang L., et al. (2021). Alignment of cellulose nanofibers: Harnessing nanoscale properties to macroscale benefits. ACS Nano 15:3646–3673. DOI:10.1021/acsnano.0c07613
- Lee K., Jeon Y., Kim D., et al. (2021). Double-crosslinked cellulose nanofiber based bioplastic films for practical applications. *Carbohydr. Polym.* 260:117817. DOI:10. 1016/j.carbpol.2021.117817
- Wang C., Zhao J., Liu L., et al. (2021). Transformation of fibrous membranes from opaque to transparent under mechanical pressing. *Engineering* 19:84–92. DOI:10. 1016/j.eng.2021.02.018
- Wang S., Li T., Chen C., et al. (2018). Transparent, anisotropic biofilm with aligned bacterial cellulose nanofibers. Adv. Funct. Mater. 28:1707491. DOI:10.1002/adfm. 201707491
- Benitez A.J., Torres-Rendon J., Poutanen M., et al. (2013). Humidity and multiscale structure govern mechanical properties and deformation modes in films of native cellulose nanofibrils. *Biomacromolecules* 14:4497–4506. DOI:10.1021/bm401451m
- 15. Yuan H., Wu J., Wang D., et al. (2021). Ultra-high-strength composite films prepared from nmmo solutions of bamboo-derived dissolving pulp and chitosan. *Ind. Crops Prod.* 170:113747. DOI:10.1016/j.indcrop.2021.113747
- Su H., Wang B., Sun Z., et al. (2022). High-tensile regenerated cellulose films enabled by unexpected enhancement of cellulose dissolution in cryogenic aqueous phosphoric acid. *Carbohydr. Polym.* 277:118878. DOI:10.1016/j.carbpol.2021.118878
- Shu L., Zhang X.F., Wang Z., et al. (2022). Structure reorganization of cellulose hydrogel by green solvent exchange for potential plastic replacement. *Carbohydr. Polym.* 275:118695. DOI:10.1016/j.carbpol.2021.118695
- Gao X., Li M., Zhang H., et al. (2021). Fabrication of regenerated cellulose films by dmac dissolution using parenchyma cells via low-temperature pulping from yunnanendemic bamboos. *Ind. Crops Prod.* 160:113116. DOI:10.1016/j.indcrop.2020.113116
- Zhang Q., Chen Y., Wei P., et al. (2021). Extremely strong and tough chitosan films mediated by unique hydrated chitosan crystal structures. *Mater. Today* 51:27–38. DOI:10.1016/j.mattod.2021.10.030
- Hu L., Zhong Y., Wu S., et al. (2021). Biocompatible and biodegradable supertoughness regenerated cellulose via water molecule-assisted molding. *Chem. Eng. J.* 417:129229. DOI:10.1016/j.cej.2021.129229
- Tu H., Zhu M., Duan B., et al. (2020). Recent progress in high-strength and robust regenerated cellulose materials. Adv. Mater. 33:2000682. DOI:10.1002/adma. 202000682
- Ismail N., Venault A., Mikkola J.P., et al. (2020). Investigating the potential of membranes formed by the vapor induced phase separation process. *J. Membr. Sci.* 597:117601. DOI:10.1016/j.memsci.2019.117601
- 23. Zhao Q., Xie R., Luo F., et al. (2018). Preparation of high strength poly(vinylidene fluoride) porous membranes with cellular structure via vapor-induced phase separation. *J. Membr. Sci.* **549**:151–164. DOI:10.1016/j.memsci.2017.10.068
- Chae Park H., Po Kim Y., Yong Kim H., et al. (1999). Membrane formation by water vapor induced phase inversion. *J. Membr. Sci.* 156:169–178. DOI:10.1016/S0376-738 8(98)00359-7
- Wang Q., Nnanna P.C., Shen F., et al. (2021). Full utilization of sweet sorghum for bacterial cellulose production: A concept of material crop. *Ind. Crops Prod.* 162:113256. DOI:10.1016/j.indcrop.2021.113256
- 26. International A. (2013). Standard test method for intrinsic viscosity of cellulose.
- Ye D., Lei X., Li T., et al. (2019). Ultrahigh tough, super clear, and highly anisotropic nanofiber-structured regenerated cellulose films. ACS Nano 13:4843–4853. DOI:10. 1021/acsnano.9b02081
- Kotov N., Raus V. and Dybal J. (2018). Intermolecular interactions in N,N-dimethylacetamide without and with LiCl studied by infrared spectroscopy and quantum chemical model calculations. *J. Phys. Chem. B.* 122:8921–8930. DOI:10. 1021/acs.jpcb.8b05569
- 29. Alexowsky C., Bojarska M. and Ulbricht M. (2019). Porous poly(vinylidene fluoride)

- membranes with tailored properties by fast and scalable non-solvent vapor induced phase separation. *J. Membr. Sci.* **577**:69–78. DOI:10.1016/j.memsci.2019.01.033
- 30. Ripoche A., Menut P., Dupuy C., et al. (2002). Poly(ether imide) membrnae formation by water vapour induced phase inversion. *Macromol. Symp.* **188**:37–48. DOI:10.1002/1521-3900(200211)188:1<37::AID-MASY37>3.0.CO;2-4
- Zhang C., Liu R., Xiang J., et al. (2014). Dissolution mechanism of cellulose in N, N-dimethylacetamide/lithium chloride: Revisiting through molecular interactions. *J. Phys. Chem. B.* 118:9507–9514. DOI:10.1021/jp506013c
- Wang S., Yu L., Jia X., et al. (2024). Cellulose nanofibril-guided orienting response of supramolecular network enables superstretchable, robust, and antifatigue hydrogel. *Innov. Mater.* 2:100092. DOI:10.59717/j.xinn-mater.2024.100092
- Moon R.J., Martini A., Nairn J., et al. (2011). Cellulose nanomaterials review: Structure, properties and nanocomposites. *Chem. Soc. Rev.* 40:3941–3994. DOI:10.1039/ cocsonings
- Sugiyama J., Vuong R. and Chanzy H. (1991). Electron diffraction study on the two
  crystalline phases occurring in native cellulose from an algal cell wall.

  Macromolecules 24:4168–4175. DOI:10.1021/ma00014a033
- 35. Nogi M., Iwamoto S., Nakagaito A.N., et al. (2009). Optically transparent nanofiber paper. *Adv. Mater.* **21**:1595–1598. DOI:10.1002/adma.200803174
- Hou Y., Guan Q.F., Xia J., et al. (2021). Strengthening and toughening hierarchical nanocellulose via humidity-mediated interface. ACS Nano 15:1310–1320. DOI:10. 1021/acsnano.0c08574
- 37. Ritchie R.O. (2011). The conflicts between strength and toughness. *Nat. Mater.* 10:817–822. DOI:10.1038/nmat3115
- Evans A.G. (1990). Perspective on the development of high-toughness ceramics. J. Am. Ceram. Soc. 73:187–206. DOI:10.1111/j.1151-2916.1990.tb06493.x
- 39. Launey M.E. and Ritchie R.O. (2009). On the fracture toughness of advanced materials. Adv. Mater. 21:2103–2110. DOI:10.1002/adma.200803322
- Cheng J., Chen Z., Zhou J., et al. (2018). Influences of layer thickness on the compatibility and physical properties of polycarbonate/polystyrene multilayered film via nanolayer coextrusion. *Appl. Surf. Sci.* 440:946–954. DOI:10.1016/j.apsusc.2018. 01.254
- Zhang X., Liu W., Liu W., et al. (2020). High performance pva/lignin nanocomposite films with excellent water vapor barrier and UV-shielding properties. *Int. J. Biol. Macromol.* 142:551–558. DOI:10.1016/j.ijbiomac.2019.09.129
- Ku H., Wang H., Pattarachaiyakoop N., et al. (2011). A review on the tensile properties of natural fiber reinforced polymer composites. *Compos. Part B: Eng.* 42:856–873. DOI:10.1016/j.compositesb.2011.01.010
- Yamane C., Aoyagi T., Ago M., et al. (2006). Two different surface properties of regenerated cellulose due to structural anisotropy. *Polym. J. (Tokyo, Jpn.)* 38:819–826. DOI:10.1295/polymj.PJ2005187
- Ma Q., Wang K., Mohawk D., et al. (2021). Strong, ductile, transparent, water-resistant cellulose nanofibril composite films via UV-induced inter-cross-linked networks. ACS Sustainable Chem. Eng. 9:10749–10760. DOI:10.1021/acssuschemenq.1c01222
- 45. Wei P., Huang J., Lu Y., et al. (2019). Unique stress whitening and high-toughness double-cross-linked cellulose films. *ACS Sustainable Chem. Eng.* **7**:1707–1717. DOI:10.1021/acssuschemeng.8b05485
- Liu S., Zeng J., Tao D., et al. (2010). Microfiltration performance of regenerated cellulose membrane prepared at low temperature for wastewater treatment. *Cellulose* 17:1159–1169. DOI:10.1007/s10570-010-9450-6
- 47. Martins R., Barquinha P., Pereira L., et al. (2008). Write-erase and read paper memory transistor. *Appl. Phys. Lett.* **93**:203501. DOI:10.1063/1.3030873
- 48. Zhu H., Xiao Z., Liu D., et al. (2013). Biodegradable transparent substrates for flexible

- organic-light-emitting diodes. *Energy Environ. Sci.* **6**:2105–2111. DOI:10.1039/C3EE40492G
- Nogi M., Komoda N., Otsuka K., et al. (2013). Foldable nanopaper antennas for origami electronics. *Nanoscale* 5:4395–4399. DOI:10.1039/C3NR00231D
- Zhu H., Fang Z., Preston C., et al. (2014). Transparent paper: Fabrications, properties, and device applications. Energy Environ. Sci. 7:269–287. DOI:10.1039/C3EE43024C

#### FUNDING AND ACKNOWLEDGMENTS

This work was financially supported by the Canada First Research Excellence Fund, National Natural Science Foundation of China (No. 22176031), Shanghai Natural Science Foundation (21ZR426200), the Program for Professor of Special Appointment (Eastern Scholar) at Shanghai Institutions of Higher Learning, Science Foundation of National Innovation Center of Advanced Dyeing and Finishing Technology (2022GCJJ22), the Opening Project of Jiangsu Engineering Research Center of Textile Dyeing and Printing for Energy Conservation, Discharge Reduction and Cleaner Production (ERC) (Grant number: SDGC2430) and National Natural Science Foundation of China (51703123). We gratefully acknowledge Poland's high-performance computing infrastructure PLGrid (HPC Centers: ACK Cyfronet AGH) for providing computer facilities and support within computational grant no. PLG/2023/016884 and the financial support of the National Science Centre, Poland (2019/35/B/ST4/01149 OPUS 18). The funders had no role in study design, data collection and analysis, decision to publish, or preparation of the

#### **AUTHOR CONTRIBUTIONS**

H.Z. conceived the initial idea for this study, designed the experiments, performed the measurements and developed it further with the support of J.G.H. and Z.S.C. G.C.H., B.A. and Q.W. was heavily involved in sample fabrication confirming initial concepts, assisted in experimental design. Q.W. performed the DP of all samples and analyzed all XRD measurements. G.C.H. performed the large-scale fabrication of samples. B.A. performed the biocompatibility and biodegradability test of samples. P.B. and W.P. performed and analyzed all molecular modeling calculations. Q.S.T performed the life-cycle assessment. F.S. was involved in sample fabrication confirming initial concepts and provided valuable discussions. N.Z., L.H.X. and Q.Y. provided valuable discussion. H.Z. drafted the manuscript with the support of J.G.H., W.P. and Z.S.C, and the manuscript was written through contributions of all authors. All authors reviewed and commented on the paper. All authors contributed to the manuscript and approved the final version.

## **DECLARATION OF INTERESTS**

The authors declare no competing interests.

#### DATA AND CODE AVAILABILITY

The authors declare that the main data supporting the findings of this study are available within the paper and its Supplemental Information. Extra data are available on reasonable request from the corresponding author.

### SUPPLEMENTAL INFORMATION

It can be found online at https://doi.org/10.59717/j.xinn-mater.2025.100133